Tetrahedron 66 (2010) 8949–8957

Contents lists available at ScienceDirect

Tetrahedron

journal homepage: www.elsevier.com/locate/tet

Conformational study of the natural iron chelator *myo*-inositol 1,2,3-trisphosphate using restrained/flexible analogues and computational analysis

David Mansell [a], Nicolás Veiga [b], Julia Torres [b], Laura L. Etchells [a], Richard A. Bryce [a], Carlos Kremer [b], Sally Freeman [a,*]

[a] School of Pharmacy & Pharmaceutical Sciences, University of Manchester, Oxford Road, Manchester, M13 9PT, UK
[b] Cátedra de Química Inorgánica, Departamento Estrella Campos, Facultad de Química, Universidad de la República, CC 1157, Montevideo, Uruguay

ARTICLE INFO

Article history:
Received 9 June 2010
Received in revised form 19 August 2010
Accepted 13 September 2010
Available online 17 September 2010

Keywords:
myo-Inositol 1,2,3-trisphosphate
Iron chelation
Chair conformation
Inositol phosphates
Computational analysis

ABSTRACT

myo-Inositol 1,2,3-trisphosphate [Ins(1,2,3)P_3], a component in mammalian cells, possesses the correct chemical properties of an intracellular iron transit ligand. Here we have examined the conformation of the Ins(1,2,3)P_3–Fe^{3+} complex. The synthesis and antioxidant properties of 4,6-carbonate-*myo*-inositol 1,2,3,5-tetrakisphosphate [4,6-carbonate Ins(1,2,3,5)P_4], which is locked in the unstable penta-axial chair conformation and 1,2,3-trisphosphoglycerol, a flexible acyclic analogue of Ins(1,2,3)P_3, are reported. 4,6-Carbonate Ins(1,2,3,5)P_4 caused complete inhibition of iron-catalysed hydroxyl radical (HO•) formation at 100 μM, thereby resembling Ins(1,2,3)P_3 and supporting a penta-axial chair binding conformation. In contrast, 1,2,3-trisphosphoglycerol was shown to have incomplete antioxidant properties. In support of experimental observations, we have applied high-level density functional calculations to the binding of Ins(1,2,3)P_3 to iron. This study provides evidence that Fe^{3+} binds tightly to the less stable penta-axial conformation of Ins(1,2,3)P_3 using terminal and bridging phosphate oxygens, thought to also contain a tightly bound water molecule or hydroxyl ligand in the complex.

1. Introduction

myo-Inositol 1,2,3-trisphosphate [Ins(1,2,3)P_3, **1**] and other 1,2,3-trisphosphate containing *myo*-inositol phosphates possess remarkable iron chelation and antioxidant properties.[1–4] We have recently shown that **1**, a cellular component in a variety of mammalian cells, possesses the correct chemical properties expected of an intracellular iron transit ligand.[5] That is, (i) the capacity to associate with iron to the full stoichiometric extent even in the presence of cellular amounts of Mg^{2+}, (ii) the capacity to maintain such full association with iron in acidic and/or Ca^{2+}-rich compartments, and (iii) the capacity to inhibit iron redox cycling and associated production of free radicals. This final property is unique to the *myo*-inositol phosphates containing the 1,2,3-trisphosphate motif, and is crucial given the dangers associated with iron-catalysed free radical formation. The binding conformation of Ins(1,2,3)P_3, and more specifically the orientation of the phosphate groups around iron, is key to the binding of iron in a 'safe' manner. Ins(1,2,3)P_3 can exist in two chair conformations, orientating the phosphate groups either equatorial–axial–equatorial (**1A**) or axial–equatorial–axial (**1B**) (Scheme 1). The crystal structure of the cyclohexylammonium salt of Ins(1,2,3)P_3,[6] showed the expected stable penta-equatorial chair conformation. Using a pyrene-based fluorescent probe, we have recently demonstrated that Ins(1,2,3)P_3 undergoes a ring-flip from the penta-equatorial (**1A**, **1a5e**) to the penta-axial chair conformation (**1B**, **5a1e**) upon association with Fe^{3+} (Scheme 1).[7,8] This result is consistent with the Ins(1,2,3)P_3–Fe^{3+} structure proposed by Phillippy and Graf, in which the *myo*-inositol chair adopts the penta-axial conformation with hexa-coordination of iron by two terminal oxygens from each phosphate group.[9] This binding geometry was proposed following an observation that the inhibition of Fe^{3+}-catalysed hydroxyl radical formation by a ligand typically arises from the occupation of all six coordination sites around iron, thus preventing its participation in the Haber–Weiss redox cycles.[10]

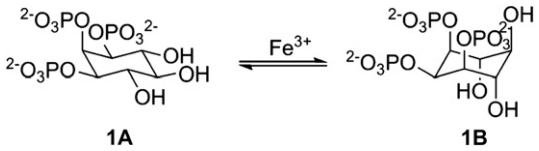

Scheme 1. Conformational ring-flip of Ins(1,2,3)P_3 from the penta-equatorial (**1A**) to the penta-axial chair (**1B**) upon association with Fe^{3+}.

* Corresponding author. Tel.: +44 161 275 2366; fax: +44 161 275 2396; e-mail address: sally.freeman@manchester.ac.uk (S. Freeman).

0040-4020/$ – see front matter © 2010 Elsevier Ltd. All rights reserved.
doi:10.1016/j.tet.2010.09.033

Here, we extend the analysis of the Ins(1,2,3)P_3–Fe^{3+} complex with the design of conformationally restricted Ins(1,2,3)P_3 analogues, which are locked in the penta-axial chair conformation by either a methylene (**2**) or carbonate bridge (**3**) between the 4,6-hydroxyl groups (Fig. 1). The methylene acetal displays particularly high stability towards acidic cleavage, making it an ideal candidate for a conformational lock. Alternatively, the cyclic carbonate protecting group has previously been used by Angyal to lock the *myo*-inositol chair in its unstable penta-axial conformation.[11] In addition, 1,2,3-trisphosphoglycerol (**4**), a flexible acyclic analogue of Ins(1,2,3)P_3 (**1**) (Fig. 1), has been synthesised to probe the role of the rigid cyclohexane framework in the binding of iron. The straight-chain trisphosphoglycerol (**4**) structure could mimic the conformation of the 1,2,3-trisphosphate motif, but lacks the rotational restriction of the cyclohexane ring, allowing considerable flexibility of the phosphate groups.

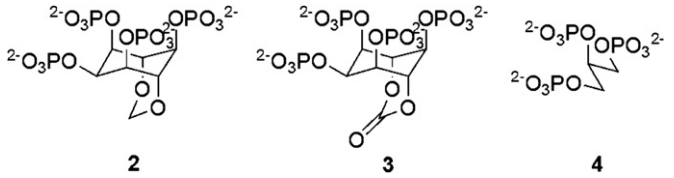

Fig. 1. Conformationally restricted (**2**) and (**3**), and acyclic (**4**) analogues of Ins(1,2,3)P_3 (**1**).

The extent to which these analogues are able to bind iron and inhibit Fe^{3+}-catalysed hydroxyl radical formation should provide evidence for the binding conformation of the 1,2,3-trisphosphate motif to Fe^{3+}. These experimental observations are supported using high-level density functional calculations of the Ins(1,2,3)P_3–Fe^{3+} complex.

2. Results and discussion

2.1. Synthesis of the conformationally restricted penta-axial analogues (2) and (3)

The initial aim was to prepare conformationally restricted analogues of Ins(1,2,3)P_3 (**1**), which are locked in the energetically less stable penta-axial conformation by a short bridging group between the 4,6-diaxial hydroxyl groups. However, a conformationally restricted *myo*-inositol 1,2,3,5-tetrakisphosphate analogue, possessing an additional P5 phosphate group, was chosen as a more feasible synthetic target. The *myo*-inositol 1,2,3,5-tetrakisphosphate analogue was also employed in our pyrene-based fluorescent probe and its Fe(III) chelation properties indicated that a 1,2,3,5-tetrakisphosphate analogue was a good model for the 1,2,3-trisphosphate motif.[7,8]

The primary target was 4,6-methylene-*myo*-inositol 1,2,3,5-tetrakisphosphate (**2**) (Fig. 1), which is locked in the penta-axial chair conformation by a 4,6-bridging methylene acetal. The synthesis of **2** started from *myo*-inositol (**5**), which was locked into the penta-axial conformation by protection with an orthoformate group to give **6**.[12] Selective silylation on the equatorial hydroxyl group of **6** gave diol **7**.[11] The methylene acetal was introduced by slow addition of dibromomethane:50% aqueous NaOH (1:1) and cetyl-NMe_3Br to a solution of **7** in DCM to give **8** (Scheme 2).[13–15] Hydrolysis of the orthoformate and silyl groups in **8** was achieved in the presence of *p*-toluenesulfonic acid to give **9**. Phosphorylation of tetraol **9** with dibenzyl *N*,*N*-diisopropylphosphoramidite, followed by oxidation with *m*-chloroperoxybenzoic acid gave tetrakisphosphate **10**, albeit in a surprisingly low yield (3%). In addition to the desired product, a small amount of hexaphosphorylated *myo*-inositol was also formed, which may indicate that the methylene bridge was labile under the phosphorylation conditions. Alternatively the low yield may have resulted from incomplete phosphorylation, however, we were unable to identify any further products by flash column purification. Furthermore, benzyl deprotection of **10** by catalytic hydrogenolysis was inconclusive, therefore the synthesis of the methylene analogue (**2**) could not be pursued further. Consequently, the synthesis of the 4,6-carbonate analogue (**3**) was proposed as an alternative.

Pentasodium 4,6-carbonate-*myo*-inositol 1,2,3,5-tetrakisphosphate (**3**) was synthesised via diol **7** (Scheme 2). The cyclic carbonate bridge was introduced between the 4,6-diaxial hydroxyl groups by reacting **7** with 1,1′-*O*-carbonyldiimidazole at 65–70 °C in anhydrous THF to give the fully protected **11**.[11] Selective deprotection of an orthoformate group in a 4,6-carbonate-*myo*-inositol based co-polymer has been reported using *p*-toluenesulfonic acid

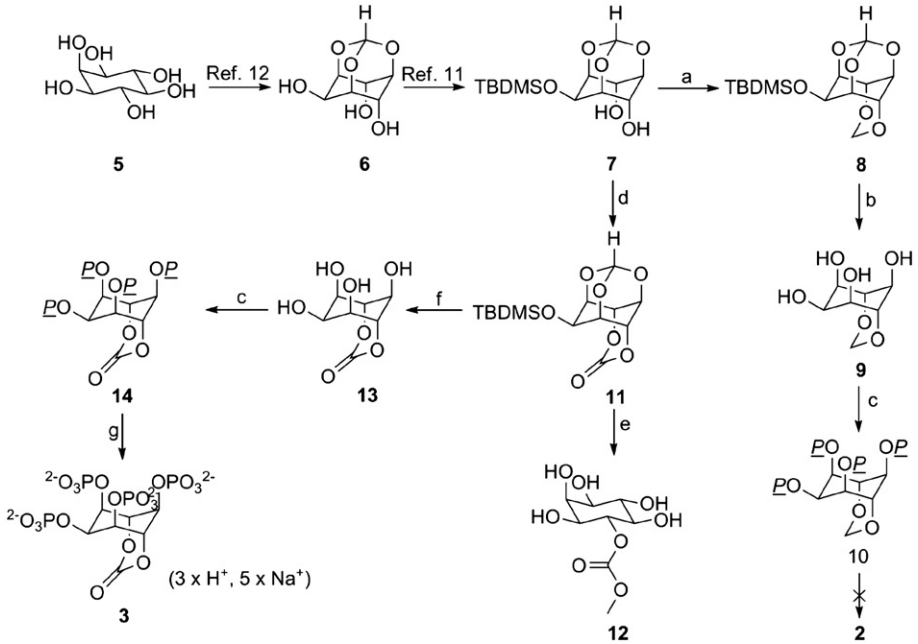

Scheme 2. Synthetic approaches towards the conformationally restricted analogues (**2**) and (**3**): (a) CH_2Br_2:50% NaOH (aq) (1:1), cetyl-Me_3NBr, CH_2Cl_2; (b). Chloroform/methanol (2:1), *p*TsOH; (c) $(BnO)_2PNPr^i_2$, 0.45 M 1*H*-tetrazole in MeCN, then *m*CPBA in anhydrous CH_2Cl_2; (d) 1,1′-*O*-carbonyldiimidazole, anhydrous THF, 65–70 °C; (e) *p*-toluenesulfonic acid, THF/MeOH (2:1); (f) 80% trifluoroacetic acid (aq), 65–70 °C; (g) H_2, Pd/C (10%), THF. *P*=$(BnO)_2P(O)$–.

in a THF/methanol solution at room temperature.[16] Using these conditions, however, the deprotection of the orthoformate and TBDMS groups in **11** was accompanied by partial cleavage of the carbonate bridge, due to nucleophilic attack by methanol generating 4-(methoxycarbonyl)-*myo*-inositol (**12**). Carbonate **12** was evident from the ^{1}H NMR spectrum, with a singlet for the methoxy group at δ 3.82 ppm and large $J_{ax/ax}$ coupling constants for the inositol protons due to the penta-equatorial conformation. A procedure for the simultaneous deprotection of the orthoformate and silyl groups in **11** is described by Angyal using aqueous trifluoroacetic acid at 65–70 °C,[11] however, under these conditions the deprotection was accompanied by the formation of some *myo*-inositol due to cleavage of the carbonate group.[11] Here, deprotection of **11** using these conditions gave tetraol **13** contaminated with a small amount of *myo*-inositol, which could be removed via hot filtration with acetonitrile. Pure 4,6-carbonate-*myo*-inositol (**13**) was obtained in an 83% yield. Phosphorylation of tetraol **13** proceeded smoothly to give the tetrakisphosphate **14**. Benzyl deprotection of **14** was achieved by catalytic hydrogenation to generate the free acid, which was converted to the sodium salt (**3**) on a Dowex cation-exchange column.

2.2. Synthesis of 1,2,3-trisphosphoglycerol (4)

Despite an extensive literature search, the synthesis of 1,2,3-trisphosphoglycerol (**4**) has not been reported. A search on the pharmacogenomics databases, Kyoto Encyclopedia of Genes and Genomes (KEGG) and Human Metabolome Database (HMDB), did not detect **4** by mass spectrometry, suggesting that it is not a natural product. The most direct route to synthesise 1,2,3-trisphosphoglycerol (**4**) would be to simultaneously phosphorylate the three hydroxyl groups of glycerol (Scheme 3). However, attempted phosphorylation of glycerol with dibenzyl *N*,*N*-diisopropylphosphoramidite in the presence of 1*H*-tetrazole in acetonitrile, followed by oxidation with *m*CPBA did not provide phosphate triester **18**. Several unidentified products, which could not be separated by flash column chromatography, were formed. In contrast, 1,2,3-trisphosphoglycerol **4** was readily prepared utilising commercially available 1,2-isopropylidene glycerol (**19**, R=H) (Scheme 3). Phosphorylation of **19** (R=H) gave **20** [R=(O)P(OBn)$_2$], followed by cleavage of the isopropylidene acetal to give diol **21**.[17] Further phosphorylation of the diol afforded an efficient route to phosphate triester **18**. Catalytic hydrogenolysis of **18** to remove the benzyl groups gave 1,2,3-trisphosphoglycerol (**4**), isolated as its tetrasodium salt.

Pentasodium *myo*-inositol 1,2,3,5-tetrakisphosphate [Ins(1,2,3,5)P$_4$, **15**] was synthesised by phosphorylation of 4,6-dibenzyl-*myo*-inositol (**16**), via the phosphate ester (**17**), following a modified route described by Šala and co-workers (Scheme 4).[18] This provides a standard, alongside Ins(1,2,3)P$_3$, to which the iron chelation properties of the conformationally restricted (**3**) and acyclic (**4**) analogues can be compared. The iron binding properties of Ins(1,2,3,5)P$_4$ (**15**) have previously been reported,[1] however the potassium salt was used[19] and the assay conditions were slightly different to those employed here.[1]

2.3. Inhibition of iron-catalysed hydroxyl radical formation

The inhibition of iron-catalysed hydroxyl radical formation by Ins(1,2,3)P$_3$ (**1**), *myo*-inositol 1,2,3,5-tetrakisphosphate (**15**), 4,6-carbonate-*myo*-inositol 1,2,3,5-tetrakisphosphate (**3**) and 1,2,3-trisphosphoglycerol (**4**) was studied using an assay for the Haber–Weiss reaction. *myo*-Inositol 1,2,6-trisphosphate [Ins(1,2,6)P$_3$] was also included in the study to illustrate the behaviour of inositol phosphates lacking the 1,2,3-trisphosphate grouping. The assay conditions were based on those described by Hawkins and co-workers[4] and Graf and co-workers,[10,3] utilising a hypoxanthine/xanthine oxidase system for HO$^\bullet$ generation. The HO$^\bullet$ generated reacts with dimethylsulfoxide (present in the assay). The first intermediate formed is the methyl radical, which reacts with O_2 to give the methylperoxy radical (Me–O–O$^\bullet$). This decomposes to form formaldehyde,[20] which is measured using the Hantzsch reaction with pentan-2,4-dione to give diacetyldihydrolutidine (absorbance at 410 nm).[21] The quantity of formaldehyde produced reflects the ability of the *myo*-inositol phosphates [**1**, **15**, **3** and Ins(1,2,6)P$_3$] and 1,2,3-trisphosphoglycerol (**4**) to chelate iron and inhibit HO$^\bullet$ formation (Fig. 2).

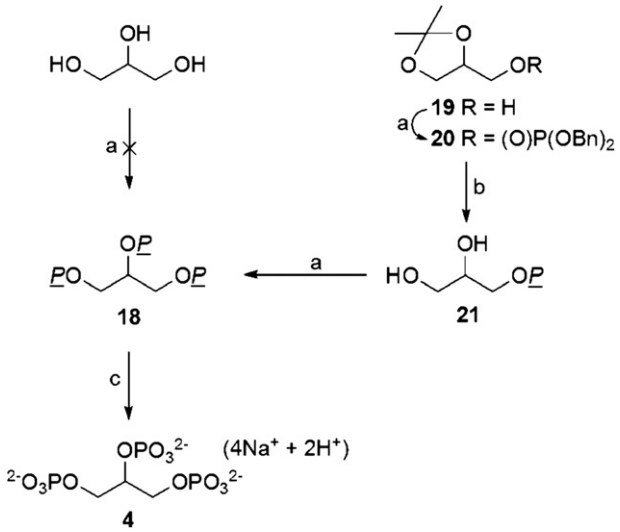

Scheme 3. Synthesis of 1,2,3-trisphosphoglycerol (**4**): (a) (BnO)$_2$PNPr$^i_2$, 0.45 M 1*H*-tetrazole in MeCN, then *m*CPBA in CH_2Cl_2; (b) Dowex-50-X8 (H^+ form), methanol; (c) H_2, Pd/C, ethanol. *P*=(BnO)$_2$P(O)$^-$.

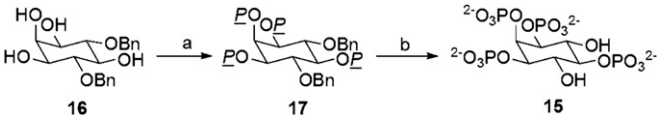

Scheme 4. Synthesis of pentasodium *myo*-inositol 1,2,3,5-tetrakisphosphate (**15**): (a) (BnO)$_2$PNPr$^i_2$, 0.45 M 1*H*-tetrazole in MeCN, then *m*CPBA in CH_2Cl_2; (b) H_2, Pd/C, ethanol. *P*=(BnO)$_2$P(O)$^-$.

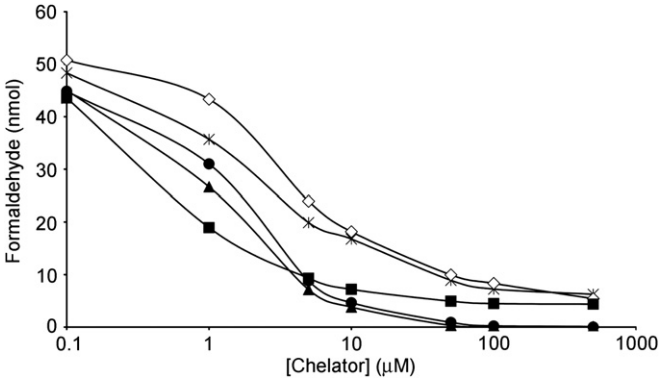

Fig. 2. Effects of Ins(1,2,3)P$_3$ (**1**, ●), Ins(1,2,3,5)P$_4$ (**15**, ▲), 4,6-carbonate-*myo*-inositol 1,2,3,5-tetrakisphosphate (**3**, ■), 1,2,3-trisphosphoglycerol (**4**, ✳) and Ins(1,2,6)P$_3$ (◇) on HO$^\bullet$ generation. The results shown are typical of three independent experiments.

Consistent with previous observations, both Ins(1,2,3)P$_3$ (**1**) and Ins(1,2,3,5)P$_4$ (**15**) completely inhibited Fe^{3+}-catalysed hydroxyl radical formation at ~100 μM.[1] For the conformationally restricted analogue, 4,6-carbonate Ins(1,2,3,5)P$_4$ (**3**), a more rapid initial decrease in HO$^\bullet$ formation was observed, compared to Ins(1,2,3)P$_3$ and

Ins(1,2,3,5)P_4, and although HO$^{\bullet}$ formation was not completely eliminated, it does reach a minimum at a concentration of ~100 μM. The iron binding properties observed for the penta-axial analogue, 4,6-carbonate Ins(1,2,3,5)P_4 (**3**), support the data obtained using the fluorescent probe 4,6-bispyrenoyl *myo*-inositol 1,2,3,5-tetrakisphosphate for the complexation of Fe^{3+} with the 1,2,3-trisphosphate motif.[7,8] In contrast, a continual reduction in HO$^{\bullet}$ formation was observed for Ins(1,2,6)P_3, which lacks the 1,2,3-trisphosphate motif. Residual HO$^{\bullet}$ formation observed for **3** could be rationalised on the basis of a second binding site being present in the molecule, in the form of the *syn*-1,3,5-triaxial trisphosphate groups (Fig. 3, **B**).[22] Iron bound at site **B** is likely to possess an available coordination site and therefore allow its participation in the Haber–Weiss cycles.

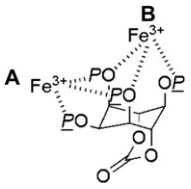

Fig. 3. Two potential Fe^{3+} binding sites are present in 4,6-carbonate-*myo*-inositol 1,2,3,5-tetrakisphosphate (**3**): at the 1,2,3-trisphosphate motif (**A**) and the *syn*-1,3,5-triaxial trisphosphate grouping (**B**).

In 1,2,3-trisphosphoglycerol (**4**), the flexibility of the phosphate groups may facilitate occupation of all coordination sites on iron. Consequently, **4** might be expected to possess similar iron chelation and antioxidant properties to Ins(1,2,3)P_3 and Ins(1,2,3,5)P_4. However, **4** was unable to completely inhibit HO$^{\bullet}$ formation and instead closely resembled the behaviour of Ins(1,2,6)P_3. Thus, it is likely that the conformational rigidity offered by the cyclohexane ring in the *myo*-inositol 1,2,3-trisphosphates facilitates effective binding of iron and may explain why nature evolved Ins(1,2,3)P_3 as an intracellular iron shuttle,[5] over the simpler 1,2,3-trisphosphoglycerol.

2.4. Computational analysis

To obtain detailed structural information, we have completed quantum mechanical calculations at the UB3LYP/6-31+G* level of theory on the high-spin Fe^{3+}–Ins(1,2,3)P_3 complex. The proposal by Graf and co-workers[10] that inhibition of Fe^{3+}-catalysed HO$^{\bullet}$ formation arises from occupation of all coordination sites around iron arose from competitive displacement experiments using an azide ligand. A relationship was observed between the presence of a free iron coordination site (i.e., occupied by water or an easily displaceable ligand) and the ability of an iron-chelate to inhibit HO$^{\bullet}$ formation. However, this result might be compatible with the presence of a tightly bound stable water molecule in the coordination sphere of Fe^{3+}. Therefore a molecule of tightly bound water may complete the coordination of iron in the Ins(1,2,3)P_3–Fe^{3+} complex. Accordingly, we have extended our high-level quantum mechanical calculations on the Ins(1,2,3)P_3–Fe^{3+} complex to include a water molecule.

*2.4.1. Comparison between penta-axial (**5a1e**) and penta-equatorial (**1a5e**) conformations of Ins(1,2,3)P_3.* The penta-axial (**5a1e**) and penta-equatorial (**1a5e**) *myo*-inositol conformations of Ins(1,2,3)P_3 in the absence of Fe^{3+} were first compared. In Fig. 4, the electrostatic potential was mapped on to an isodensity surface for the completely ionised form (L^{6-}) of both conformers. The most negative zones are shown in red and the least negative in blue. In both cases, the optimised geometries show that a hydrogen bond occurs between the phosphate group at position 2 and one OH on C4 (**5a1e** conformation) or C5 (**1a5e** conformation). For **1a5e** (Fig. 4A), this bond is strong enough to produce a little structural distortion, leading the carbon ring conformation to become closer to a boat

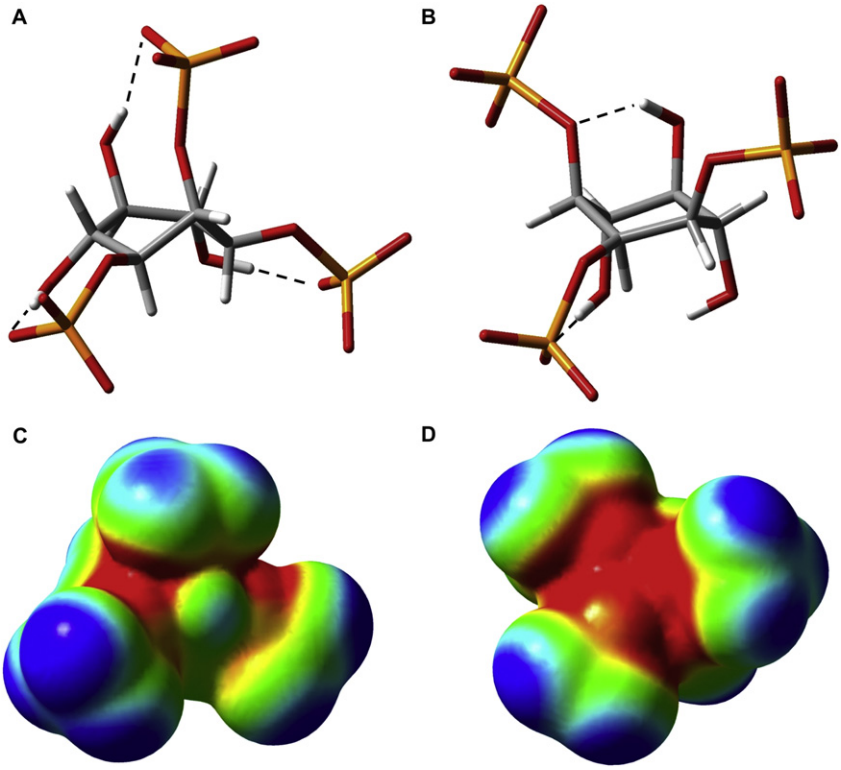

Fig. 4. (A) Penta-equatorial (**1a5e**) and (B) penta-axial (**5a1e**) conformations of In(1,2,3)P_3 in the absence of Fe^{3+}. (C) and (D) correspond to the electrostatic potential of (A) and (B) mapped on to an isodensity surface (isodensity value=0.0004 e, UB3LYP/6-31+G* geometries). The strongest intramolecular hydrogen bonds are shown as dashed lines.

rather than a chair. As it is exposed, this conformation has the most negatively charged zones between the phosphate groups, and a less negatively charged zone (due to the hydrogen atom at position 2) pointing towards the position where the metal ion will be bound (Fig. 4C). In contrast, the **5a1e** L^{6-} conformation has a 'pre-formed' geometry for metal complexation, as its most negatively charged zones are arranged in a 'hole', which can bind Fe^{3+} without significant structural distortion (Fig. 4D). It seems that the **5a1e** conformation of the L^{6-} species has a geometry that is suitable to complex the metal ion without a drastic change in the structure. This was in support of our experimental observations; consequently, we focused our computational study on the penta-axial conformation of the Ins(1,2,3)P_3–Fe^{3+} complex (Fig. 5).

2.4.2. Penta-axial conformation of Ins(1,2,3)P_3-Fe^{3+}. Initially, conformational analysis of the penta-axial conformation of the [Ins(1,2,3)P_3–Fe]$^{3-}$ was performed using the UB3LYP/LANL2DZ level, prior to exploration at the UB3LYP/6-31+G* level. Similar structures were obtained from both models, showing that there is no macroscopic difference in the geometry as the method level increases. In fact, the average bond distance between the metal ion and the donor atoms of the ligands, D(Fe–X), for both structures, are almost identical at 2.08 Å (LANL2DZ) and 2.09 Å (6-31+G*). The optimal UB3LYP/6-31+G* geometry obtained is shown in Fig. 5A. In contrast to the structure suggested by Phillippy and Graf,[9] our structure predicts the involvement of both terminal oxygens and bridging phosphoester oxygens from each phosphate. This results in a strongly distorted octahedral geometry around iron. The six Fe–O bond distances are: 2.20 Å (Fe–O1), 1.94 Å (Fe–O2), 2.10 Å (Fe–O3), 1.98 Å (Fe–O4), 2.44 Å (Fe–O5) and 1.88 Å (Fe–O6). The O1–Fe–X angles, which highlight the distortion of this octahedron, are: 70.7° (X=O2), 74.7° (X=O3), 144.0° (X=O4), 70.0° (X=O5) and 100.0° (X=O6).

2.4.3. With one coordinated water molecule. In order to cover all possibilities for the coordination of Ins(1,2,3)P_3–Fe^{3+} by a water molecule, four configurations of the complex were explored at the UB3LYP/LANL2DZ level. In three out of four optimised configurations, a hydroxide group linked to the metal centre is formed, with Ins(1,2,3)P_3 protonated. The most stable geometry from this study was used for UB3LYP/6-31+G* calculations. The optimal UB3LYP/6-31+G* structure (Fig. 5B) differs slightly in metal coordination environment compared to that obtained at the UB3LYP/LANL2DZ level: the iron moves away from O1, changing the Fe–O1 bond distance from 2.27 Å (LANL2DZ) to 2.92 Å (6-31+G*). This effect can be explained by means of the diffuse functions contained in the Gaussian basis set used, which, in general, supports the existence of weaker and longer chemical bonds through the space. In addition, this result also gives an appreciation of the non-negligible volume occupied by the OH group, which distorts to some extent the metal coordination environment. Particularly interesting is the observed proton transfer from the water molecule to the 2-phosphate group of Ins(1,2,3)P_3, which confers extra stability due to the formation of a hydrogen bond $O_W\cdots H_W O2$ (Fig. 5B). This $O_W\cdots H_W$ distance is 1.80 Å, while the O2-$H_W\cdots O_W$ angle is 176.9° and the $H_W\cdots O_W$-Fe angle is 115.3°.

The mean Fe–X distance, D(Fe–X), for [FeL(H_2O)]$^{3-}$ at the UB3LYP/LANL2DZ level is the same as that obtained for the anhydrous complex (2.08 Å, Table 1). However, for the 6-31+G* geometry, the mean Fe–X distance is longer when water is added (2.16 Å,

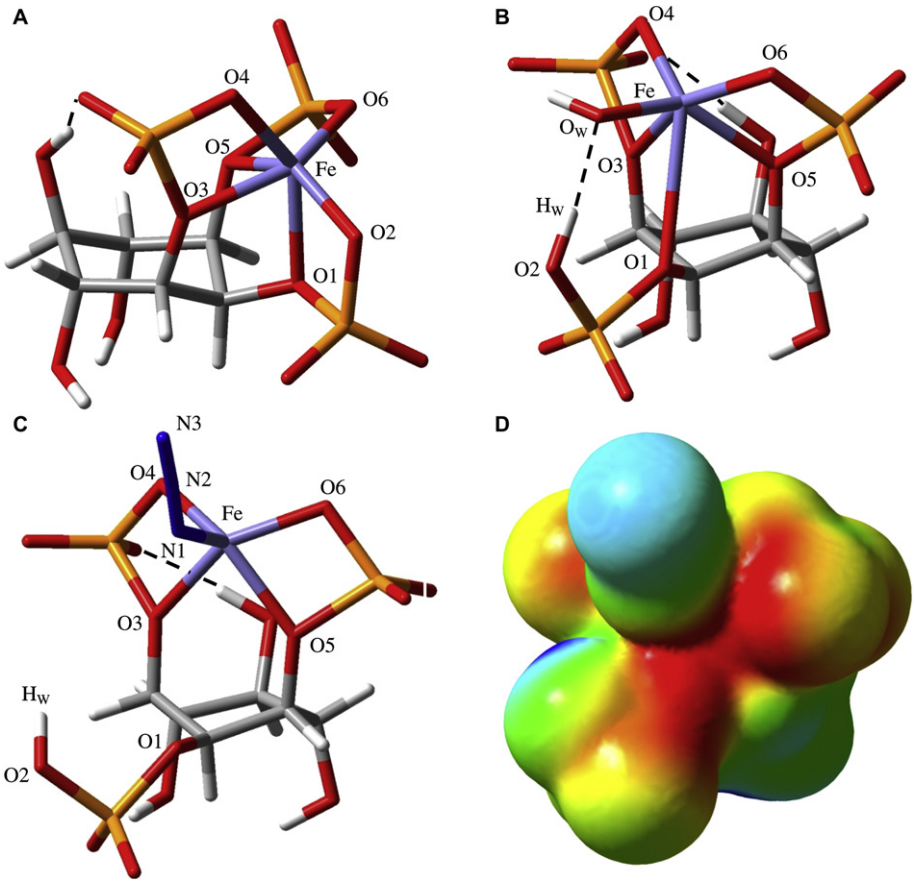

Fig. 5. Penta-axial conformation of Ins(1,2,3)P_3 bound to Fe^{3+} in: (A) the absence of water, (B) the presence of water, and (C) the presence of azide. The strongest intramolecular hydrogen bonds are shown as dashed lines. In (D), the electrostatic potential is mapped on to an isodensity surface for (C, [FeHLN_3]$^{3-}$). Isodensity value=0.0004 e, UB3LYP/6-31+G* geometry.

Table 1), due to the previously mentioned distortion that surrounds the Fe(III). Taking into account only the five shorter Fe–X bonds found in the complex, the mean bond distance is 2.00 Å. This shows that increasing the Fe–O1 bond length allows the other chelating atoms to approach the metal ion more closely. Indeed, the HO^- ligand is now 0.05 Å closer than in the UB3LYP/LANL2DZ structure.

Table 1
Mean distances (D) for UB3LYP/LANL2DZ and UB3LYP/6-31+G* optimised structures of $[FeL(H_2O)]^{3-}$. X refers to the donor chelating O atoms, either from hydroxide or phosphate

	$[FeL(H_2O)_n]^{3-}$	D(Fe–X) (Å)	D(Fe–OH) (Å)
UB3LYP/6-31+G*	n=0	2.09[a]	—
UB3LYP/LANL2DZ	n=1	2.08[a]	1.94
UB3LYP/6-31+G*	n=1	2.16[a]	1.89
		2.00[b]	

[a] D(Fe–X) averaged over all six Fe–X bonds.
[b] D(Fe–X) averaged over the five shorter Fe–X bonds.

Using the calculated absolute values of Gibbs free energies, we can compute the ΔG for the reaction involving the addition of one water molecule (Eq. 1). The addition of one water molecule to [Ins(1,2,3)P_3–Fe]$^{3-}$ is predicted to be energetically favourable (at least in the gas phase), with an exothermic ΔG of −17.4 kcal/mol (LANL2DZ) and −11.4 kcal/mol (6-31+G*).

$$[FeL]^{3-} + H_2O \rightarrow [FeL(H_2O)]^{3-} \quad (1)$$

2.4.4. Water displacement by an azide ion. After consideration of the observations by Graf and co-workers,[10] we have evaluated the displacement of the Fe-bound hydroxyl ligand from $[FeL(H_2O)]^{3-}$ by azide (Eq. 2). The calculated ΔG of reaction at the UB3LYP/6-31+G* level show that this reaction is certainly not spontaneous, with an endothermic ΔG of + 33.9 kcal/mol.

$$\left[FeL(H_2O)^{3-}\right] + N_3^- \rightarrow [FeHLN_3]^{3-} + OH^- \quad (2)$$

Inspection of the optimised geometries for $[FeL(H_2O)]^{3-}$ and $[FeHLN_3]^{3-}$ complexes suggests that substitution of HO^- by azide causes a substantial disturbance of the metal coordination sphere. In this event, the phosphate at position 2 moves away from the metal, losing the hydrogen bond with the OH^- group (Fig. 5B) and giving rise to a pentacoordinated metal environment (Fig. 5C). Accordingly, in view of the electrostatic potential of $[FeHL(azide)]^{3-}$ (Fig. 5D), it is clear that the azide group faces the most negatively charged zone, being largely repelled by adjacent groups. As a result, the phosphate in position 2 is pulled apart from the metal ion. It seems this repulsion is significant enough to prevent the expected $O2–H_W\cdots N_3^-$ hydrogen bond from forming.

Therefore, from an energetic point of view, two main factors could explain the positive ΔG value determined for displacement by azide. Firstly, this geometric deformation may be due to the electrostatic repulsion between the N_3^- ion and the phosphate groups. In contrast to what happens to the OH^- ion, the hydrogen bond cannot compensate it, and the phosphate groups are separated from each other. Secondly, the azide ion is bulkier than the hydroxyl group, the resulting steric repulsion also disfavouring substitution by azide.

3. Conclusion

We report the synthesis and antioxidant properties of conformationally restricted pentasodium 4,6-carbonate-*myo* Ins(1,2,3,5)P_4 (**3**), which models the unstable axial–equatorial–axial conformation of the 1,2,3-trisphosphate motif. Although $HO^\bullet$ formation was not completely eliminated in the presence of **3**, it does reach a minimum at a concentration of ~100 μM. This was consistent with the concentration at which Ins(1,2,3)P_3 and Ins(1,2,3,5)P_4 achieved complete inhibition of $HO^\bullet$ formation. Residual $HO^\bullet$ formation was rationalised on the basis of a second binding site for Fe^{3+} (Fig. 3, **B**) due to the *syn*-1,3,5-triaxial trisphosphate group arrangement.[22] This provides evidence that Fe^{3+} binds tightly to the penta-axial conformation of inositol phosphates possessing the 1,2,3-trisphosphate motif, consistent with previous studies with a fluorescent probe.[7,8] In contrast, 1,2,3-trisphosphoglycerol (**4**), the acyclic analogue of Ins(1,2,3)P_3, was unable to completely inhibit iron-catalysed hydroxyl radical formation, making clear the requirement for the rigid cyclohexane frame of *myo*-inositol on which the 1,2,3-trisphosphate motif features.

Density functional calculations at the UB3LYP/6-31+G* level indicate that the penta-axial conformation of Ins(1,2,3)P_3 possesses a 'pre-formed' geometry ideal for Fe^{3+} complexation. Subsequent calculations on the Ins(1,2,3)P_3–Fe^{3+} complex in the penta-axial conformation predicted a highly distorted octahedral geometry due to hexa-coordination of iron by a terminal oxygen and phosphoester oxygen from each phosphate. The inclusion of a water molecule in the coordination sphere alleviates the distortion around iron and is consequently energetically favourable. Displacement of this tightly bound water molecule with azide is energetically unfavourable, which is in agreement with experimental observations in the literature.[10] Therefore the Ins(1,2,3)P_3–Fe^{3+} complex is proposed to adopt the **5a1e** conformation which may contain a tightly bound hydroxyl ligand originating from a deprotonated water molecule.

4. Experimental

4.1. General methods

Reagents and solvents were purchased from Aldrich Chemical Co. (Dorset, UK), VWR International (Leicestershire, UK) and Fisher Scientific (Leicestershire, UK). Deuterated solvents and tetramethylsilane (TMS) were obtained from Cambridge Isotope Laboratories Inc. (Andover, USA). Thin layer chromatography was performed on pre-coated silica gel 60 F_{254} aluminium backed plates (layer thickness 0.2 mm) (Merck). Spots were visualised by ultraviolet radiation at 254 nm and 325 nm using a UV GL-58 mineral light lamp or by staining with $KMnO_4$ solution. Melting points (mp) were determined in open glass capillary tubes on a GallenKamp MPD.350.BM2.5 apparatus microscope (UK) and are uncorrected. Infra-red spectra were recorded on neat samples using a JASCO FT/IR 4100 instrument. NMR spectra were recorded using a Bruker Avance-300 spectrometer operating at 300 MHz (^{1}H NMR), 75 MHz (^{13}C NMR) or 121 MHz (^{31}P NMR) at 293 K, unless otherwise stated. The spectrometer was running TOPSPIN NMR system software (Version 2.0). Chemical shifts (δ) are reported in parts per million (ppm). ^{1}H NMR and ^{13}C NMR spectra were referenced to Me_4Si (0.00 ppm), unless otherwise stated. ^{31}P NMR spectra were referenced to 85% phosphoric acid. ^{1}H NMR spectra were assigned with the aid of COSY experiments and ^{13}C NMR spectra were assigned with the aid of DEPT experiments. Mass spectra (MS) [Micromass PLATFORM II (ES) and Thermo Finnigan MAT95XP (accurate mass)] and elemental analyses [EA 1108 Elemental Analyser (Carlo Erba Instrument)] were recorded in the School of Chemistry, University of Manchester (UK).

4.2. Synthesis

*4.2.1. Attempted synthesis of 4,6-methylene-myo-inositol 1,2,3,5-tetrakisphosphate (**2**).*

*4.2.1.1. 2-O-(tert-Butyldimethylsilyl)-4,6-methylene-myo-inositol 1,3,5-orthoformate (**8**).* A solution of 2-*O*-(*tert*-butyldimethylsilyl)-*myo*-inositol 1,3,5-orthoformate[12,11] (**7**) (1.40 g, 4.60 mmol) in DCM (80 mL) was added dropwise to a mixture of dibromomethane

(100 mL), sodium hydroxide (120 mL, 50% aq) and cetyl-trimethylammonium bromide (0.50 g, 1.38 mmol) at 65 °C, with vigorous stirring. The reaction mixture was stirred for a further 15 min and then diluted with DCM (500 mL). The organic layer was washed with water (2×50 mL) and brine (1×50 mL), dried over Na_2SO_4 and concentrated under reduced pressure. The crude material was purified by flash column chromatography (hexane/ethyl acetate, 3:1→1:1) to give **8** as a colourless solid (0.55 g, 38%). Mp 102–102.5 °C. ^{1}H NMR ($CDCl_3$): 0.15 (6H, s, $SiMe_2$), 0.94 (9H, s, ^{t}Bu), 4.08–4.17 (2H, m, H-1/3), 4.55 (1H, br s, H-2), 4.68 (1H, d, CH_AH$_B$, J_{gem} 5.9 Hz), 4.78 (2H, t, H-4/6, $^3J_{4/6-1/3} \approx {}^3J_{4/6-5}$ 4.7 Hz), 4.82–4.88 (1H, m, H-5), 5.20 (1H, d, CH$_A$$H_B$, J_{gem} 5.9 Hz), 5.48 (1H, d, H-7, $^5J_{7-2}$ 0.7 Hz). ^{13}C NMR ($CDCl_3$): −4.61 ($SiMe_2$), 18.4 (CMe_3), 25.9 (CMe_3), 61.6 (inositol CH), 61.9 (inositol CH), 66.3 (2×inositol CH), 72.3 (2×inositol CH), 84.7 (CH_2), 102.3 (C-7). MS (electrospray) *m/e* $[M+Na]^+$ 339. Anal. Calcd for $C_{14}H_{24}O_6Si$: C 53.14; H 7.65%. Found: C 52.90; H 7.64%. IR data: ν_{max} 2947 (m), 2927 (m), 2877 (m), 2857 (m) (C–H), 1255 (Si–Me), 1144 (s), 1131 (s).

*4.2.1.2. 4,6-Methylene-myo-inositol (**9**).* A solution of **8** (0.09 g, 0.28 mmol) and *p*-toluenesulfonic acid (0.03 g, 0.14 mmol) in chloroform/methanol (3 mL, 2:1) was stirred at 40 °C for 48 h. Upon cooling a precipitate formed containing a mixture of 4,6-methylene-*myo*-inositol (**9**) and a small amount of *myo*-inositol (**4**). The precipitate was filtered, washed with cold diethyl ether (3×1 mL) and the product purified by hot filtration in acetonitrile to give **9** as a colourless solid (0.04 g, 74% yield). Mp 194–196 °C. ^{1}H NMR (D_2O, referenced to DMSO at 2.71 ppm): 4.13 (2H, br t, H-1/3, $^3J_{1/3-2} \approx {}^3J_{1/3-4/6}$ 3.6 Hz), 4.36 (1H, t, H-2, $^3J_{2-1/3}$ 4.4 Hz), 4.51 (2H, t, H-4/6, $^3J_{4/6-1/3} \approx {}^3J_{4/6-5}$ 3.8 Hz), 4.68 (1H, d, CH_AH$_B$-8, J_{gem} 5.9 Hz), 4.85 (1H, t, H-5, $^3J_{5-4/6}$ 4.1 Hz), 5.17 (1H, d, CH$_A$$H_B$-8, J_{gem} 6.0 Hz). ^{13}C NMR (D_2O, referenced to DMSO at 39.4 ppm): 62.6 (inositol CH), 65.5 (inositol CH), 72.0 (2×inositol CH), 72.3 (2×inositol CH), 85.1 (CH_2). MS (electrospray +ve) *m/e* $[M+Na]^+$ 215.1; (electrospray −ve) *m/e* $[M+e]^-$ 190.9. Anal. Calcd for $C_7H_{12}O_6$: C 43.75; H 6.29%. Found: C 44.14; H 5.94%. IR data: ν_{max} 3417 (m), 3300 (m) (O–H), 2902 (w) (C–H).

*4.2.1.3. 4,6-Methylene-myo-inositol 1,2,3,5-tetrakis(dibenzyl phosphate) (**10**).* Dibenzyl *N,N*-diisopropylphosphoramidite (2.38 mL, 7.08 mmol) was added to a mixture of 4,6-methylene-*myo*-inositol (**9**) (0.17 g, 0.88 mmol) and 1*H*-tetrazole (~0.45 M solution in MeCN) (31.5 mL, 14.2 mmol). The reaction mixture was stirred under argon for 4 h at room temperature, then cooled to −40 °C. A solution of 3-chloroperoxybenzoic acid (3.0 g, ~13.5 mmol) in anhydrous DCM (80 mL) was added dropwise. The reaction mixture was stirred at 0 °C for 3 h, followed by dilution with DCM (150 mL) and then washed with 10% Na_2SO_3 (2×80 mL), satd $NaHCO_3$ (2×80 mL) and brine (1×80 mL). The organic layer was dried over $MgSO_4$, concentrated under reduced pressure and purified by flash column chromatography (hexane/ethyl acetate, 2:1→0:1) to give **10** as a colourless oil (0.03 g, 3%). ^{1}H NMR ($CDCl_3$): 4.25 (2H, br s, H-4/6), 4.57 (2H, br s, methylene–CH_2), 4.88–5.11 (20H, m, 8×P–O–CH_2Ph+H-1/3+H-2+H-5), 7.02–7.28 (40H, m, Ph). ^{13}C NMR (100 MHz, $CDCl_3$): 69.0–69.2 (m, inositol CH), 69.4 (d, J_{PC} 5.5 Hz, 2×PhCH_2OP), 69.6 (d, J_{PC} 5.9 Hz, 2×PhCH_2OP), 69.7 (d, J_{PC} 5.7 Hz, 2×PhCH_2OP), 69.9 (d, J_{PC} 5.5 Hz, 2×PhCH_2OP), 70.8–71.2 (m, inositol CH), 74.6 (br s, C-1/3), 82.8 (s, C-4/6), 104.0 (CH_2), 127.7, 128.0, 128.19, 128.23, 128.27, 128.32, 128.37, 128.43, 128.6 (all s, aromatic CH), 135.6 (d, J_{PC} 7.4 Hz, 2×Cq *Ph*CH_2OP), 135.6 (d, J_{PC} 6.6 Hz, 2×Cq *Ph*CH_2OP), 135.7 (d, J_{PC} 7.8 Hz, 4×Cq *Ph*CH_2OP). ^{31}P NMR ($CDCl_3$): −1.48 (2P), −1.19 (1P), −0.50 (1P). ^{31}P NMR ($CDCl_3$, ^{1}H-coupled): −1.50 (sextet, J_{PH} 7.5 Hz, 2P), −1.20 (dpentet, J_{PH} 11.6 Hz, J_{PH} 7.3 Hz, 1P), −0.53 (br q, J_{PH} 7.3 Hz, 1P). MS (electrospray) *m/e* $[M+Na]^+$ 1256. IR data: ν_{max} 1277 (s, P=O), 997 (P–O–Bn).

*4.2.2. Synthesis of 4,6-carbonate-myo-inositol 1,2,3,5-tetrakis-phosphate **3**.*

*4.2.2.1. 4,6-Carbonate-myo-inositol (**13**).* The deprotection of 2-*O*-*tert*-butyldimethyl-4,6-carbonate-*myo*-inositol 1,3,5-orthoformate (**11**) (0.05 g, 0.15 mmol) in the presence of *p*-toluenesulfonic acid (0.015 g, 0.08 mmol) in chloroform/methanol (2:1, 2 mL) was unsuccessful. The solution was stirred at 45 °C for 48 h and then cooled on ice. The precipitate was isolated by filtration and the colourless solid identified as 4-*O*-methoxycarbonyl-*myo*-inositol (**12**) (0.02 g, 61%). Mp 173.5–175.5 °C. ^{1}H NMR (D_2O, referenced to DMSO at 2.71 ppm): 3.47 (1H,t, H-5, $^3J_{2-1} \approx {}^3J_{2-3}$ 9.5 Hz), 3.54 (1H, dd, H-1, $^3J_{1-6}$ 9.9 Hz, $^3J_{1-2}$ 2.8 Hz), 3.70 (1H, t, H-6, $^3J_{6-1} \approx {}^3J_{6-5}$ 9.9 Hz), 3.74 (1H, dd, H-3, $^3J_{3-4}$ 10.3 Hz, $^3J_{3-2}$ 2.6 Hz), 3.82 (3H, s, MeO), 4.08 (1H, t, H-2, $^3J_{2-1} \approx {}^3J_{2-3}$ 2.8 Hz), 4.85 (1H, t, H-4, $^3J_{4-3} \approx {}^3J_{4-5}$ 9.9 Hz). ^{13}C NMR (D_2O, referenced to DMSO at 39.4 ppm): 56.1 (CH_3), 69.9 (CH, inositol), 71.6 (CH, inositol), 72.7 (CH, inositol), 72.8 (CH, inositol), 72.9 (CH, inositol), 80.0 (CH, inositol), 157.1 (C=O). MS (electrospray) *m/e* $[M+Na]^+$ 261. Accurate mass calcd for $C_8H_{14}O_8Na$: 261.0586. Found: 261.0581 (error: −2.1 ppm). IR data: ν_{max} 3328 (br) (O–H), 1721 (C=O), 1310 (C–H). 4,6-Carbonate-*myo*-inositol (**13**) was subsequently prepared according to the literature procedure.[11] Under these conditions *myo*-inositol was formed as an impurity and was removed by hot filtration in acetonitrile. Mp 171–172 °C, lit. mp 172 °C.[11] ^{1}H NMR (D_2O, referenced to acetonitrile at δ 2.06 ppm): 4.00 (1H, t, H-2, $^3J_{2-1/3}$ 4.3 Hz), 4.36–4.44 (2H, m, H-1/3), 4.58 (1H, tt, H-5, $^3J_{5-4/6}$ 3.7 Hz, $^4J_{5-1/3}$ 1.2 Hz), 4.90 (2H, t, H-4/6, $^3J_{4/6-1/3} \approx {}^3J_{4/6-5}$ 3.8 Hz).

*4.2.2.2. 4,6-Carbonate-myo-inositol 1,2,3,5-tetrakis(dibenzyl phosphate) (**14**).* The phosphorylation of **13** was achieved under the conditions described for the preparation of compound **10**. The crude residue was purified by flash column chromatography (hexane/ethyl acetate 3:1→0:1) to give **14** as a colourless oil (0.19 g, 31%). ^{1}H NMR ($CDCl_3$): 4.51–4.65 (2H, m, H-5+H-2), 4.83 (2H, t, H-4/6, $^3J_{4/6-1/3} \approx {}^3J_{4/6-5}$ 3.7 Hz), 4.89–5.11 (18H, m, H-1/3+8×P–O–CH_2–Ph), 7.05–7.36 (40H, m, Ph). ^{13}C NMR ($CDCl_3$): 64.1 (d, J_{PC} 4.3 Hz, inositol C-5), 66.5 (dt~q, $^3J_{PC} \approx {}^2J_{PC}$ 5.3 Hz, inositol C-2), 69.7 (d, J_{PC} 5.6 Hz, 2×PhCH_2OP), 70.0 (d, J_{PC} 5.9 Hz, 2×PhCH_2OP), 70.2 (d, J_{PC} 5.6 Hz, 2×PhCH_2OP), 70.4 (d, J_{PC} 5.7 Hz, 2×PhCH_2OP), 71.1 (t, J_{PC} 4.7 Hz, inositol C-4/6), 72.8 (dd, $^3J_{PC}$ 4.8 Hz, $^2J_{PC}$ 2.9 Hz, inositol C-1/3), 127.9, 128.0, 128.1, 128.2, 128.4, 128.5, 128.5, 128.7, 128.9 (all s, aromatic), 135.1 (Cq, d, J_{PC} 6.7 Hz, 2×*Ph*CH_2OP), 135.27 (Cq, d, J_{PC} 6.7 Hz, 2×*Ph*CH_2OP), 135.31 (Cq, d, J_{PC} 7.4 Hz, 2×*Ph*CH_2OP), 135.35 (Cq, d, J_{PC} 7.3 Hz, 2×*Ph*CH_2OP), 143.8 (C=O). ^{31}P NMR ($CDCl_3$): −1.45 (2P), −1.37 (1P), −0.96 (1P). ^{31}P NMR ($CDCl_3$, ^{1}H-coupled): −1.46 (sextet, J_{PH} 8.8 Hz), −1.39 (sextet, J_{PH} 8.8 Hz), −0.97 (sextet, J_{PH} 9.2 Hz). MS (electrospray) *m/e* $[M+Na]^+$ 1269.2. IR data: ν_{max} 1789 (C=O), 1092 (P–O–Bn).

*4.2.2.3. Pentasodium 4,6-carbonate-myo-inositol 1,2,3,5-tetrakis-phosphate (**3**).* A mixture of **14** (0.048 g, 0.038 mmol) and Pd–C (10%, 0.013 g) was stirred in tetrahydrofuran (10 mL) under a hydrogen atmosphere for 24 h at room temperature. The catalyst was removed by filtration through a pad of Celite and the solvent removed under reduced pressure. The residue was dissolved in water (2 mL) and the solution applied to a cation-exchange column (Dowex-50-X8, mesh 20–50, 5 mL, Na^+ form) and eluted with water (25 mL). The eluent was concentrated to approximately 3 mL and lyophilised to give **3** as a colourless solid (0.021 g, 79%). Mp >300 °C. ^{1}H NMR (500 MHz, D_2O, referenced to DMSO at 2.71 ppm): 4.47–4.54 (1H, m, H-2), 4.82–4.91 (3H, m, H-1/3+H-5), 5.16 (2H, t, H-4/6, $^3J_{4/6-1/3} \approx {}^3J_{4/6-5}$ 2.8 Hz). ^{13}C NMR (D_2O, referenced to DMSO at 39.39 ppm): 63.6 (d, J_{PC} 4.3 Hz, C-5), 66.0 (dt~q, $^2J_{PC} \approx {}^3J_{PC}$ 5.4 Hz, C-2), 70.6 (t, $^3J_{PC}$ 4.8 Hz, C-4/6), 75.4 (d, J_{PC} 4.2 Hz, C-1/3), 149.5 (C=O). ^{31}P NMR (D_2O): 1.17 (1P), 1.43 (1P), 1.51 (2P).

^{31}P NMR (D_2O, ^{1}H-coupled): 1.15 (d, J_{PH} 8.7 Hz), 1.47 (br s). Anal. Calcd for $C_7H_9O_{19}P_4Na_5.3H_2O$: C 12.18; H 2.19; P 17.96%. Found: C 12.35; H 2.29; P 17.60%. IR data: ν_{max} 3336 (br) (residual water), 1743 (C=O), 1650 (br).

*4.2.3. Synthesis of myo-inositol 1,2,3,5-tetrakisphosphate (**15**). 4.2.3.1. 4,6-Dibenzyl-myo-inositol (**16**).* *p*-Toluenesulfonic acid monohydrate (0.16 g, 0.83 mmol) was added to 2-*O*-(*tert*-butyldimethylsilyl)-4,6-dibenzyl-*myo*-inositol 1,3,5-orthoformate[11,12,23] (0.40 g, 0.83 mmol) in methanol (10 mL). The mixture was stirred at room temperature for 48 h. The reaction mixture was concentrated and the residue purified by flash column chromatography (DCM/methanol 9:1) to give **16** as a colourless solid (0.24 g, 81%). Mp 138–139 °C, lit. mp 138.5–139 °C.[24] ^{1}H NMR ($CDCl_3$): 2.60 (3H, br s, 3×OH), 2.89 (1H, br s, OH), 3.52 (2H, dd, H-1/3, $^3J_{1/3-4/6}$ 9.2 Hz, $^3J_{1/3-2}$ 2.3 Hz), 3.53 (1H, t, H-5, $^3J_{5-4/6}$ 9.5 Hz), 3.67 (2H, t, H-4/6, $^3J_{4/6-1/3} \approx {}^3J_{4/6-5}$ 9.3 Hz), 4.08 (1H, t, H-2, $^3J_{2-1/3}$ 2.6 Hz), 4.83 (2H, d, 2×O–C*H*$_A$H$_B$Ph, J_{gem} 11.4 Hz), 4.89 (2H, d, 2×O–C*H*$_A$H$_B$Ph, J_{gem} 11.4 Hz), 7.25–7.44 (10H, m).

*4.2.3.2. 4,6-Dibenzyl-myo-inositol 1,2,3,5-tetrakis(dibenzyl phosphate) (**17**).* The phosphorylation of **16** was performed as described for the preparation of compound **10**. The crude residue was purified by flash column chromatography (hexane/ethyl acetate, 3:1→0:1) to give **17** (0.42 g, 54%) as a colourless oil. ^{1}H NMR (400 MHz, $CDCl_3$): 3.93 (2H, t, H-4/6, $^3J_{4/6-1/3} \approx {}^3J_{4/6-5}$ 9.5 Hz), 4.38 (2H, tt, H-1/3, $^3J_{1/3-4/6} \approx {}^3J_{PH}$ 9.6 Hz, $^3J_{1/3-2} \approx {}^4J_{PH}$ 1.9 Hz), 4.45 (1H, q, H-5, $^3J_{5-4/6} \approx {}^3J_{PH}$ 9.3 Hz), 4.63 (2H, dd, P–O–CH_2Ph, J_{gem} 11.8 Hz, $^3J_{PH}$ 8.9 Hz), 4.67–4.88 (8H, m, 4×C*H*$_2$Ph), 4.90–5.05 (6H, m, 3×C*H*$_2$Ph), 5.12 (4H, d, 2×C*H*$_2$Ph, J_{PH} 7.6 Hz), 5.42 (1H, dt, H-2, $^3J_{PH}$ 8.5 Hz, $^3J_{2-1/3}$ 2.1 Hz), 6.95–7.00 (4H, m, Ph), 7.05–7.10 (4H, m, Ph), 7.12–7.42 (42H, m, Ph).

*4.2.3.3. Pentasodium myo-inositol 1,2,3,5-tetrakisphosphate (**15**).* Hydrogenation of compound **17** was performed as described for the preparation of **3** to give pentasodium *myo*-inositol 1,2,3,5-tetrakisphosphate (**15**) as a colourless solid in a quantitative yield. Mp >300 °C, lit. mp >300 °C.[18] ^{1}H NMR (400 MHz, D_2O, water suppression, referenced to acetone at 2.22 ppm): 3.94 (2H, t, H-4/6, $^3J_{4/6-5} \approx {}^3J_{4/6-1/3}$ 9.3 Hz), 4.00 (1H, q, H-5, $^3J_{5-4/6} \approx J_{PH}$ 8.4 Hz), 4.11 (2H, ddd ~ br t, H-1/3, $^3J_{1/3-4/6} \approx J_{PH}$ 8.8 Hz, coupling to H-2 not observed), 4.93 (1H, td, H-2, J_{PH} 9.8 Hz, $^3J_{2-1/3}$ 2.3 Hz). ^{13}C NMR (D_2O, referenced to DMSO at 39.39 ppm): 71.4 (dd, C-4/6, $^3J_{PC}$ 6.4 Hz, $^3J_{PC}$ 3.4 Hz), 74.8 (dd, C-1/3, $^2J_{PC}$ 5.2 Hz, $^3J_{PC}$ 2.8 Hz), 75.5 (d, C-5, J_{PC} 5.8 Hz), 79.3 (d, C-2, $^2J_{PC}$ 6.3 Hz, $^3J_{PC}$ not observed). ^{31}P NMR (D_2O): 0.34 (3P), 0.98 (1P). ^{31}P NMR (D_2O, ^{1}H-coupled): 0.35 (br s), 0.98 (d, J_{PH} 4.8 Hz). Anal. Calcd for $C_6H_{11}O_{18}P_4Na_5 \cdot 4H_2O$: C 10.57; H. 2.81; P 18.17. Found: C 10.90; H. 2.79; P 17.78%.

*4.2.4. Synthesis of 1,2,3-trisphosphoglycerol (**4**). 4.2.4.1. 1-(Dibenzyl phospho)-2,3-isopropylidene glycerol (**20**).* The phosphorylation of **19** was performed as described for the preparation of compound **10**. The crude residue was purified by flash column chromatography (hexane/ethyl acetate+1% triethylamine 3:1→1:1) to give **20** as a colourless oil (0.26 g, 86%). ^{1}H NMR (500 MHz, $CDCl_3$): 1.33 (3H, s, CH_3), 1.38 (3H, s, CH_3), 3.73 (1H, dd, C*H*$_A$H$_B$-3, J_{gem} 8.5 Hz, $^3J_{3-2}$ 5.5 Hz), 3.93 (1H, ddd ~ dt, C*H*$_A$H$_B$-1, J_{gem} 11.2 Hz, $J_{PH} \sim {}^3J_{1-2}$ 6.4 Hz), 3.96–4.00 (1H, m, 1×CH$_A$*H*$_B$-1), 4.01 (1H, dd, CH$_A$*H*$_B$-3, J_{gem} 6.2 Hz, $^3J_{3-2}$ 4.7 Hz), 4.21 (1H, pentet, H-2, $^3J_{2-1} \approx {}^3J_{2-3}$ 5.8 Hz), 5.04 (2H, dd, 2×P–O–C*H*$_A$H$_B$Ph, J_{gem} 11.6 Hz, J_{PH} 8.4 Hz), 5.07 (2H, dd, 2×P–O–CH$_A$*H*$_B$Ph, J_{gem} 11.6, J_{PH} 8.3 Hz), 7.31–7.39 (10H, m, 2×Ph).

*4.2.4.2. 1-(Dibenzyl phospho)glycerol (**21**).* Compound **21** was prepared according to the literature procedure.[17] The crude residue was purified by flash column chromatography (ethyl acetate) to give **21** as a colourless oil (0.34 g, 96%). ^{1}H NMR (500 MHz, $CDCl_3$): 3.19 (2H, s, 2×OH), 3.56 (1H, dd, J_{gem} 11.6 Hz, $^3J_{3A-2}$ 5.2 Hz, C*H*$_A$H$_B$-3), 3.61 (1H, dd, J_{gem} 11.6 Hz, $^3J_{3B-2}$ 4.3 Hz, CH$_A$*H*$_B$-3), 3.82 (1H, pentet, $^3J_{2-1} \approx {}^3J_{2-3}$ 5.0 Hz, H-2), 4.03 (2H, dd, J_{PH} 9.0 Hz, $^3J_{1-2}$ 5.3 Hz, CH$_2$-1), 5.02 (2H, dd, J_{gem} 11.4 Hz, J_{PH} 7.5 Hz, 2×P–O–C*H*$_A$H$_B$Ph), 5.05 (2H, dd, J_{gem} 11.4 Hz, J_{PH} 7.8 Hz, 2×P–O–CH$_A$*H*$_B$Ph), 7.30–7.40 (10H, m, Ph). ^{13}C NMR ($CDCl_3$): 62.7 (CH$_2$-3), 68.6 (d, J_{PC} 5.9 Hz, CH$_2$-1), 69.7 (d, J_{PC} 5.5 Hz, 2×PhCH$_2$OP), 70.6 (d, J_{PC} 6.1 Hz, CH-2), 128.0 (Ph), 128.6 (Ph) 128.7 (Ph), 135.5 (d, J_{PC} 6.7 Hz, 2×quat. *Ph*CH$_2$OP). ^{31}P NMR ($CDCl_3$): 0.56 (1P). ^{31}P NMR ($CDCl_3$, ^{1}H-coupled): 0.56 (1P, septet, J_{PH} 8.3 Hz).

*4.2.4.3. 1,2,3-Tris(dibenzyl phospho)glycerol (**18**).* The phosphorylation of **21** was performed as described for the preparation of compound **10**. The crude residue was purified by flash column chromatography (hexane/ethyl acetate 2:1→1:2) to give **18** as a colourless oil (0.44 g, 60%). ^{1}H NMR (500 MHz, $CDCl_3$): 4.02 (2H, ddd ~ dt, J_{gem} 11.2 Hz, $J_{PH} \sim {}^3J_{HH}$ 5.6 Hz, C*H*$_A$H$_B$-1, C*H*$_A$H$_B$-3), 4.09 (2H, ddd ~ dt, J_{gem} 11.0 Hz, $J_{PH} \sim {}^3J_{HH}$ 5.4 Hz, CH$_A$*H*$_B$-1, CH$_A$*H*$_B$-3), 4.55 (1H, dpentet, J_{PH} 9.1 Hz, $^3J_{2-1/3}$ 4.5 Hz, H-2), 4.94–5.03 (12H, m, 6×P–O–C*H*$_2$Ph), 7.22–7.34 (30H, m, Ph). ^{13}C NMR ($CDCl_3$): 65.5 (t, J_{PC} 4.9 Hz, 2×CH$_2$-1/3), 69.6 (br d, J_{PC} 5.6 Hz, 3×PhCH$_2$OP), 74.6 (td, $^3J_{PC}$ 8.7 Hz, $^2J_{PC}$ 5.3 Hz, CH-2), 128.0 (Ph), 128.1 (Ph), 128.6 (br s, Ph), 128.7 (br s, Ph), 135.7 (br d, J_{PC} 6.7 Hz, 3×quat. *Ph*CH$_2$OP). ^{31}P NMR ($CDCl_3$): −1.01 (2P, P-1/3), −1.68 (1P, P-2). ^{31}P NMR ($CDCl_3$, ^{1}H-coupled), −1.01 (2P, septet, J_{PH} 7.6 Hz, P-1/3), −1.69 (1P, sextet, J_{PH} 7.9 Hz, P-2). MS (electrospray) *m*/*e* [M+Na]$^+$ 895. Accurate mass calcd for $C_{45}H_{47}O_{12}P_3Na$: 895.2173. Found 895.2176 (error: 0.4 ppm). IR data: ν_{max} 1266 (s, P=O), 992 (P–O–Bn).

*4.2.4.4. Tetrasodium 1,2,3-trisphosphoglycerol (**4**).* Hydrogenation of compound **18** was performed as described for the preparation of **3** to give tetrasodium 1,2,3-trisphosphoglycerol (**4**) as a hydroscopic gum (0.11 g, quantitative yield). ^{1}H NMR (D_2O, referenced to acetone at 2.22 ppm): 4.39 (1H, dpentet, J_{PH} 9.6 Hz, $^3J_{2-1/3}$ 4.8 Hz, H-2), 4.07–3.94 (4H, m, CH$_2$-1/3). ^{13}C NMR (D_2O, referenced to acetone at 30.9): 64.7 (t, $^2J_{CP} \approx {}^3J_{CP}$ 4.7 Hz, CH$_2$-1/3), 73.9 (dt, $^2J_{CP}$ 8.1 Hz, $^3J_{CP}$ 5.1 Hz, CH-2). ^{31}P NMR (D_2O): 1.38 (s, P-1/3), 0.53 (s, P-2). ^{31}P NMR (D_2O, ^{1}H-coupled): 1.38 (br s, P-1/3), 0.53 (d, J_{PH} 8.1 Hz, P-2). Anal. Calcd for $C_3H_7P_3O_{12}Na_4 \cdot 4H_2O$: C 7.32; H 3.07; P 18.89%. Found: C 7.36%, H 3.53%, P 18.79%. IR data: ν_{max} 3357 (br, residual water), 1684 (br, residual water), 1184 (m, P=O).

4.3. Hydroxyl radical assay

Ultra-violet (UV) absorbance spectra were recorded on a ThermoSpectronic Unicam-300 spectrophotometer (UK) running Vision 32 software (version 1.25), using disposable 1.5 mL semi-micro cuvettes (path length 1 cm). The assay conditions employed were based on literature described by Hawkins and co-workers[4] and Graf and co-workers.[10,3] The standard assay mixture contained: 20 mM Trizma (Sigma) buffered to pH 7.5 with HCl, 50 mM dimethylsulfoxide, 0.3 mM hypoxanthine, 5 μM $FeCl_3$ (added from a freshly prepared 50 μM stock solution) and 18 m-units of xanthine oxidase (Sigma; lyophilised powder from bovine milk). For the stock hypoxanthine solution, addition of 0.1 M NaOH solution prior to dilution with buffer was required to aid solubility. For each measurement, triplicate 1.0 mL samples were prepared containing the assay mixture and varying concentrations of chelator (added from 1 mM stock solution). The fractions were incubated at 37 °C for 30 min, and then quenched by immersion in a boiling-water bath for 2 min, followed by addition of 250 μL formaldehyde detection reagent (prepared from 15 g of ammonium acetate, 0.3 mL of acetic acid and 0.2 mL of acetylacetone in a final volume of 100 mL of water). The fractions were incubated at 37 °C for 40 min to develop the colour attributed to the formation of

diacetyldihydrolutidine, and the absorbance measured at 410 nm. The blanks were incubated with heat-inactivated enzyme.

4.4. Computational methods

The current density functional theoretical study focuses on fully deprotonated Ins(1,2,3)P_3 and its high-spin Fe^{3+} complexes, using the hybrid UB3LYP functional.[25,26] The basis sets LANL2DZ[27] and 6-31+G* were applied throughout this work. All geometry optimisations were performed via the modified GDIIS algorithm in gas phase as implemented in Gaussian 03.[28] The effect of the solvent was studied through a discrete model with one water molecule. The final structures obtained were all minima in the potential energy surface, the nature of the stationary points being verified through vibrational analysis. ZPE and thermochemical corrections derived from this analysis were used to compute free energies at 298 K.

Acknowledgements

EPSRC and the School of Pharmacy and Pharmaceutical Sciences are thanked for a studentship and PhD+ award (D.M.). N.V. is indebted to PEDECIBA-Química and ANII for a scholarship. We thank Professor Christopher J. Barker (Karolinska Institutet) and Dr. Rick Dunn (The University of Manchester).

References and notes

1. Spiers, I. D.; Barker, C. J.; Chung, S.-K.; Chang, Y.-T.; Freeman, S.; Gardiner, J. M.; Hirst, P. H.; Lambert, P. A.; Michell, R. H.; Poyner, D. R.; Schwalbe, C. H.; Smith, A. W.; Solomons, K. R. H. *Carbohydr. Res.* **1996**, *282*, 81–99.
2. Spiers, I. D.; Freeman, S.; Poyner, D. R.; Schwalbe, C. H. *Tetrahedron Lett.* **1995**, *36*, 2125–2128.
3. Graf, E.; Empson, K. L.; Eaton, J. W. *J. Biol. Chem.* **1987**, *262*, 11647–11650.
4. Hawkins, P. T.; Poyner, D. R.; Jackson, T. R.; Letcher, A. J.; Lander, D. A.; Irvine, R. F. *Biochem. J.* **1993**, *294*, 929–934.
5. Veiga, N.; Torres, J.; Mansell, D.; Freeman, S.; Dominguez, S.; Barker, C. J.; Diaz, A.; Kremer, C. *J. Biol. Inorg. Chem.* **2009**, *14*, 51–59.
6. Spiers, I. D.; Freeman, S.; Schwalbe, C. H. *J. Chem. Soc., Chem. Commun.* **1995**, 2219–2220.
7. Mansell, D.; Rattray, N.; Etchells, L. L.; Schwalbe, C. H.; Blake, A. J.; Bichenkova, E. V.; Bryce, R. A.; Barker, C. J.; Diaz, A.; Kremer, C.; Freeman, S. *Chem. Commun.* **2008**, 5161–5163.
8. Mansell, D.; Rattray, N.; Etchells, L.L.; Schwalbe, C.H.; Blake, A.J.; Torres, J.; Kremer, C.; Bichenkova, E.V.; Barker, C.J.; Freeman, S. *Org. Biomol. Chem.* **2010**, *8*, 2850–2858.
9. Phillippy, B. Q.; Graf, E. *Free Radic. Biol. Med.* **1997**, *22*, 939–946.
10. Graf, E.; Mahoney, J. R.; Bryant, R. G.; Eaton, J. W. *J. Biol. Chem.* **1984**, *259*, 3620–3624.
11. Angyal, S. J. *Carbohydr. Res.* **2000**, *325*, 313–320.
12. Praveen, T.; Shashidhar, M. S. *Carbohydr. Res.* **2001**, *330*, 409–411.
13. Norman, D. G.; Reese, C. B.; Serafinowska, H. T. *Synthesis* **1985**, 751–754.
14. Kim, K. S.; Szarek, W. A. *Synthesis* **1978**, 48–50.
15. Nicolaou, K. C.; Mitchell, H. J.; Fylaktakidou, K. C.; Rodriguez, R. M.; Suzuki, H. *Chem.—Eur. J.* **2000**, *6*, 3116–3148.
16. Kim, T.-H.; Holmes, A. B. *J. Korean Chem. Soc.* **2006**, *50*, 129–136.
17. Ryan, M.; Smith, M. P.; Vinod, T. K.; Lau, W. L.; Keana, J. F. W.; Griffith, O. H. *J. Med. Chem.* **1996**, *39*, 4366–4376.
18. Šala, M.; Kolar, J.; Strlič, M.; Kočevar, M. *Carbohydr. Res.* **2006**, *341*, 897–902.
19. Chung, S.-K.; Chang, Y.-T. *J. Chem. Soc., Chem. Commun.* **1995**, 11–12.
20. Klein, S. M.; Cohen, G.; Cederbaum, A. I. *Biochemistry* **1981**, *20*, 6006–6012.
21. Nash, T. *Biochem. J.* **1953**, *55*, 416–421.
22. Volkmann, C. J.; Chateauneuf, G. M.; Pradhan, J.; Bauman, A. T.; Brown, R. E.; Murthy, P. P. N. *Tetrahedron Lett.* **2002**, *43*, 4853–4856.
23. Lee, H. W.; Kishi, Y. *J. Org. Chem.* **1985**, *50*, 4402–4404.
24. Laumen, K.; Ghisalba, O. *Biosci. Biotechnol. Biochem.* **1994**, *58*, 2046–2049.
25. Becke, A. D. *J. Chem. Phys.* **1993**, *98*, 5648–5652.
26. Lee, C.; Yang, W.; Parr, R. G. *Phys. Rev. B: Condens. Matter* **1988**, *37*, 785–789.
27. Hay, P. J.; Wadt, W. R. *J. Chem. Phys.* **1985**, *82*, 270–283.
28. Frisch, M.J.; Trucks, G.W.; Schlegel, H.B.; Scuseria, G.E.; Robb, M.A.; Cheeseman, J.R.; Montgomery, J.A.; Vreven, T.; Kudin, K.N.; Burant, J.C.; Millam, J.M.; Iyengar, S.S.; Tomasi, J.; Barone, V.; Mennucci, B.; Cossi, M.; Scalmani, G.; Rega, N.; Petersson, G.A.; Nakatsuji, H.; Hada, M.; Ehara, K.; Toyota, K.; Fukuda, R.; Hasegawa, J.; Ishida, T.; Nakajima, Y.; Honda, Y.; Kitao, O.; Nakai, H.; Klene, M.; Li, X.; Knox, J.E.; Hratchian, H.P.; Cross, J.B.; Adamo, C.; Jaramillo, J.; Gomperts, R.; Stratmann, R.E.; Yazyev, O.; Austin, A.J.; Cammi, R.; Pomelli, C.; Ochterski, J.; Ayala, P.Y.; Morokuma, K.; Voth, G.A.; Salvador, P.; Dannenberg, J.J.; Zakrzekski, V.G.; Dapprich, S.; Daniels, A.D.; Strain, M.C.; Farkas, O.; Malick, D.K.; Rabuck, A. D.; Raghavachari, K.; Foresman, J.B.; Ortiz, J.V.; Cui, Q.; Baboul, A.G.; Clifford, S.; Cioslowski, J.; Stefanov, B.B.; Liu, G.; Liashenko, A.; Piskorz, P.; Komaromi, I.I.; Martin, R.L.; Fox, D.J.; Keith, T.; Al-Laham, M.A.; Peng, C.Y.; Nanayakkara, A.; Challacombe, M.; Gill, P.M.W.; Johnson, B.G.; Chen, W.; Wong, M.W.; Gonzalez, C.; Pople, J.A. *Gaussian 03, revision B.01*, Gaussian Inc.: Pittsburgh, PA, 2003.